J Solid State Electrochem (2012) 16:83–88
DOI 10.1007/s10008-010-1277-4

ORIGINAL PAPER

Preparation and electrochemical properties of $Nd_{2-x}Sr_xFeO_{4+\delta}$ cathode materials for intermediate-temperature solid oxide fuel cells

Weimin Guo · Hongyu Liang · Junyan Pei · Chao Jin · Jiang Liu

Received: 13 November 2010 / Revised: 7 December 2010 / Accepted: 10 December 2010 / Published online: 4 January 2011

Abstract Cathodic materials $Nd_{2-x}Sr_xFeO_{4+\delta}$ (x=0.5, 0.6, 0.8, 1.0) with K_2NiF_4-type structure, for use in intermediate-temperature solid oxide fuel cells (IT-SOFCs), have been prepared by the glycine–nitrate process and characterized by XRD, SEM, AC impedance spectroscopy, and DC polarization measurements. The results have shown that no reaction occurs between an $Nd_{2-x}Sr_xFeO_{4+\delta}$ electrode and an $Sm_{0.2}Gd_{0.8}O_{1.9}$ electrolyte at 1,200 °C, and that the electrode forms a good contact with the electrolyte after sintering at 1,000 °C for 2 h. In the series $Nd_{2-x}Sr_xFeO_{4+\delta}$ (x=0.5, 0.6, 0.8, 1.0), the composition $Nd_{1.0}Sr_{1.0}FeO_{4+\delta}$ shows the lowest polarization resistance and cathodic overpotential, 2.75 Ω cm^2 at 700 °C and 68 mV at a current density of 24.3 mA cm^{-2} at 700 °C, respectively. It has also been found that the electrochemical properties are remarkably improved the increasing Sr content in the experimental range.

Keywords Intermediate-temperature solid oxide fuel cells · $Nd_{2-x}Sr_xFeO_{4+\delta}$ cathode materials · Electrochemical properties

Introduction

Solid oxide fuel cells (SOFCs) are the most efficient devices among the energy technologies hitherto devised for the conversion of chemical fuels directly into electrical power [1, 2]. The development of intermediate-temperature (600–800 °C) SOFCs (IT-SOFCs) is attracting increasing interest because they can be fabricated from a wider range of materials resulting from widening the materials chosen and are associated with decreased material degradation, prolonged lifetimes, and reduced costs, which may accelerate the commercialization of SOFCs [3]. However, a major issue that stems from the reduced operating temperature is the decrease in the catalytic activity of the cathode for oxygen reduction [4]. Therefore, many efforts are focused on reducing the operating temperature without decreasing the cell efficiency. The most promising cathode materials are mixed ionic electronic conducting (MIEC) oxides. Most of the studies on MIEC cathodes have focused on perovskites, such as $BaCoO_3$ and $LaCoO_3$ [5, 6].

Recently, a family of compounds of the form K_2NiF_4 (or A_2BO_4), with a perovskite-related structure, has attracted attention for use as MIEC cathodes due to favorable characteristics. They show good electronic conductivity attributable to the mixed valence of the B site metal and good oxygen ionic transport properties due to the oxygen overstoichiometry [7–10]. They also show thermal expansion coefficients ($10.5–14.2\times10^{-6}$ K^{-1}) comparable to those of the commonly used solid electrolytes [9, 11, 12]. Therefore, A_2BO_4 materials have been mainly used as oxygen separators, oxygen sensors, and low-temperature superconductors [13]. At present, these oxides are being extensively reexamined with regard to their possible use as cathode materials for IT-SOFCs.

Among K_2NiF_4-type A_2BO_4 compounds for potential application in SOFC cathodes, several previous studies have been focused on $Ln_2NiO_{4+\delta}$-based materials, where Ln is usually some rare earth element, most frequently La, Pr, Nd, or Sm [14–19]. It has been reported that Sr doping

W. Guo (✉) · H. Liang · J. Pei
Department of Biological and Chemical Engineering,
Guangxi University of Technology,
Liuzhou 545006, People's Republic of China
e-mail: guoweimin8@163.com

C. Jin · J. Liu
School of Chemistry and Engineering,
South China University of Technology,
Guangzhou 510640, People's Republic of China

can improve the p-type electrical conductivity of $La_{2-x}Sr_xNiO_{4+\delta}$ nickelates [20], and different kinds of oxygen defects can be formed, depending on the Sr dopant concentration [21]. It is generally believed that these oxygen defects offer the possibility of rapid oxygen transport through the ceramic material. Similar results have been obtained for Sr-doped $A_{2-x}A'_xBO_{4+\delta}$ (A=La, Pr, Sm, Nd; A′=Sr; B=Fe, Co, Cu) [12, 22–24]. Another group of compounds that possess the same structure and also contain excess oxygen are the materials $Ln_2FeO_{4+\delta}$ (Ln= La, Ba). Jin et al. [25] reported that Sr doping in Ba_2FeO_4 could improve its cathodic properties. They found that single-phase K_2NiF_4-type structures were obtained for $Ba_{2-x}Sr_xFeO_{4+\delta}$ over the composition range of $0.5 \le x \le 1.0$ for Ba. To the best of our knowledge, there has not hitherto been any report on Nd metal in the A site of $Ln_{2-x}Sr_xFeO_{4+\delta}$ materials in the literature. Therefore, the investigation and evaluation of the potential of new materials of the type $Nd_{2-x}Sr_xFeO_{4+\delta}$ as cathode materials for IT-SOFCs is very interesting.

In the present study, materials of the $Nd_{2-x}Sr_xFeO_{4+\delta}$ ($0.5 \le x \le 1.0$) series have been synthesized and characterized. In order to extend our research work, the electrochemical properties of these Sr-doped Nd_2FeO_4 materials supported on $Sm_{0.2}Gd_{0.8}O_{1.9}$ (SDC)-based electrolyte have also been studied.

Experimental

Preparation and characterization of the materials

Single-phase $Nd_{2-x}Sr_xFeO_{4+\delta}$ (x=0.5, 0.6, 0.8, 1.0) powders were prepared using the glycine–nitrate combustion process [26]. Stoichiometric amounts of analytical grade $Nd(NO_3)_3{\cdot}6H_2O$, $Sr(NO_3)_2$, and $Fe(NO_3)_3{\cdot}9H_2O$ were dissolved together in deionized water. Glycine was then added to the solution in a 2:1 molar ratio with respect to the total amount of metal ions. The solution was heated to ignition on a hot plate to obtain a powder precursor. The final powders were obtained after calcination in air at 1,000 °C for 10 h. The obtained materials are denoted, for example, as NSF1010 for $Nd_{1.0}Sr_{1.0}FeO_{4+\delta}$, NSF1505 for $Nd_{1.5}Sr_{0.5}FeO_{4+\delta}$, and so on. SDC powder was prepared by a nitrate–citrate process followed by calcination at 800 °C for 2 h [27]. SDC powder was first pressed uniaxially at 500 MPa to form a pellet and then sintered at 1,400 °C for 4 h.

The structures and phase stabilities of the materials were characterized by X-ray powder diffraction (XRD) using a Shimadzu XD-3A diffractometer ($Cu - K_\alpha$ radiation, operated at 35 kV, 30 mA, λ=0.15406 nm). The selected 2θ range was from 20 to 80º, scanning at a step size of 0.02º. The morphologies and microstructures of the sintered electrodes were examined with a Philips XL-30FEG scanning electron microscope (SEM).

Fabrication and measurement of half-cells

A typical three-electrode method was used for electrochemical characterization of the $Nd_{2-x}Sr_xFeO_{4+\delta}$ cathodes on an SDC electrolyte in air. The $Nd_{2-x}Sr_xFeO_{4+\delta}$ powders were mixed with an ethylcellulose–terpineol vehicle to form an ink, which was subsequently painted on one side of the SDC pellet to form a working electrode with an area of 0.35 cm^2. Silver paste was painted on the other side of the pellet in a symmetrical configuration as the counter electrode. A silver wire was used as reference electrode (RE) and put on the same side of the working electrode. The RE was normally placed at 3–5 mm from the working electrode, ensuring that this distance was at least three times the thickness of the electrolyte. A silver grid was applied to the surface of the cathode by painting with silver paste, which served as the final current collector. The cathodes were first heated at 400 °C for 2 h to eliminate organic binders, and then sintered at 950–1,100 °C for 2 h in air, with a heating/cooling rate of 5 °C min^{-1}. Electrochemical impedance spectroscopy (EIS) and steady-state polarization measurements of the half-cells were performed using an Autolab PGSTAT30 (Holland) electrochemical analyzer. For the steady-state polarization measurements of the half-cells, IR compensation was carried out by the interruption method to eliminate the ohmic polarization. EIS measurements were performed in the frequency range 100 kHz to 0.1 Hz with a signal amplitude of 10 mV under open-circuit conditions at 500–700 °C.

Results and discussion

Characterization of the powders

Figure 1 shows the XRD patterns of prepared $Nd_{2-x}Sr_xFeO_{4+\delta}$ (x=0.5, 0.6, 0.8, 1.0) after sintering at 1,000 °C for 10 h. Samples with x=0.5, 0.6, 1.0 basically crystallized in a single phase with K_2NiF_4 structure, while sample with x=0.8 shows a small amount of impurity peaks, which can be indexed as NdO_2. Reaction between the electrode and electrolyte is of course undesirable for the long-term stability of SOFCs. Hence, the reactivity of NSF1010 with the SDC electrolyte was further studied. Figure 2 shows the XRD pattern of a mixture of NSF1010 and SDC powders in a weight ratio of 1:1 after heat treatment at 1,200 °C for 24 h, along with those of the individual components. It was observed that the structures of NSF1010 and SDC remained unchanged. No new peaks or shifts of XRD peaks were discernible in the pattern

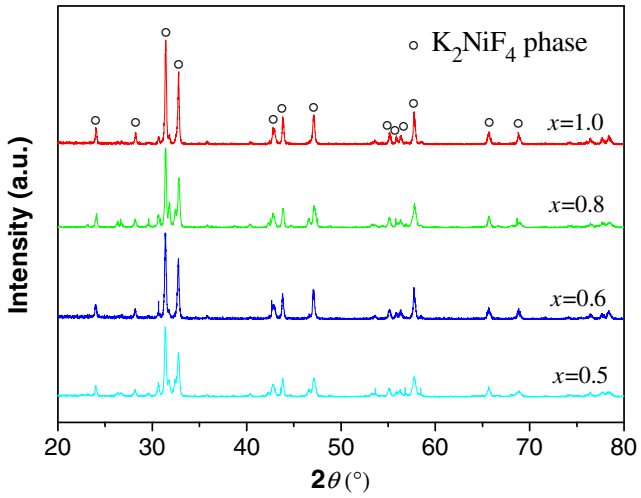

Fig. 1 XRD patterns of $Nd_{2-x}Sr_xFeO_{4+\delta}$ (x=0.5, 0.6, 0.8, 1.0) sintered at 1,000 °C for 10 h in air

(Fig. 2), indicating that no reaction and/or inter-diffusion of elements occurred between NSF1010 and SDC within the XRD method resolution range. This result revealed that NSF1010 had good chemical compatibility with the SDC electrolyte in the experimental range.

Electrochemical measurements of the cathode material

In order to investigate the effect of sintering temperature on the NSF cathode properties, a number of different sintering conditions were studied. NSF1010 cathodes were sintered at 950, 1,000, and 1,100 °C for 2 h, and then the EIS was measured at 700 °C in air. The results are presented in Fig. 3. The impedance spectra were fitted using the equivalent circuit $R_E(R_1\text{CPE1})(R_2\text{CPE2})$ shown in Fig. 3 (see inset), which is given by the measuring system. The

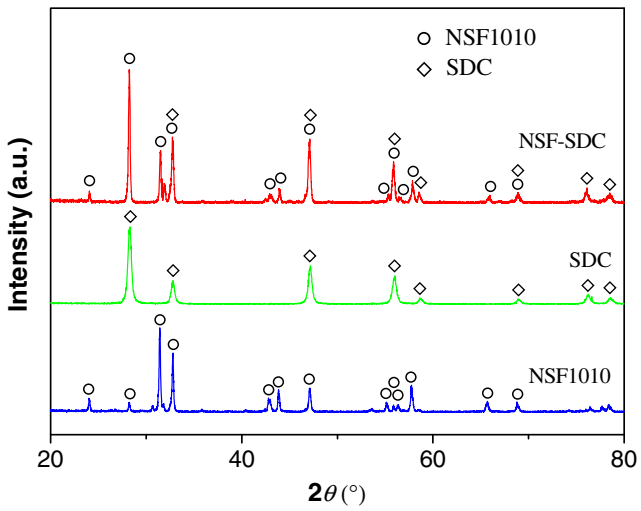

Fig. 2 XRD patterns of $Nd_{1.0}Sr_{1.0}FeO_{4+\delta}$ –SDC mixture sintered at 1,200 °C for 24 h in air

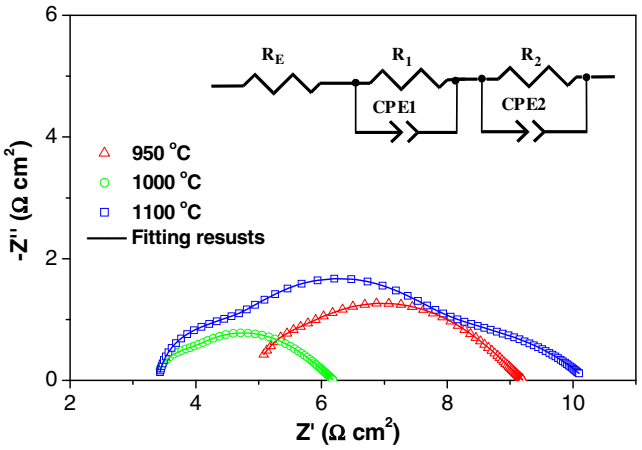

Fig. 3 Impedance spectra under open-circuit potential at 700 °C in air of NSF1010 cathodes sintered at 950–1,100 °C for 2 h

intercepts of the impedance arcs with the real axis at high frequencies correspond to the overall ohmic resistance, which comprises the electrolyte resistance, electrode (including anode and cathode) ohmic resistance, and the contact resistance between electrode, current collector, and lead wires, while the overall size of the arcs can be attributed to cathode polarization resistance (R_p). Two impedance arcs are observed at low and high frequencies, which indicates that there are at least two electrode processes limiting the oxygen reduction reaction. The resistance at high frequency corresponds to the charge–transfer resistance (R_1), which is contributed by the electrochemical reaction at the electrode/electrolyte interface, while that at the low-frequency arc is attributed to the oxygen adsorption or desorption process on the electrode surface and the diffusion of oxygen ions (R_2) [28, 29]. The total cathodic R_p is the sum of R_1 and R_2. CPE1 and CPE2 are the corresponding constant phase elements [30]. It was found that the sintering temperature had a remarkable effect on the electrode performance. From the impedance spectra, it was observed that the electrode polarization was relatively high after sintering at 950 °C. R_p attained its lowest value at 1,000 °C, and then increased once more when the sintering temperature was increased to 1,100 °C.

As is well known, the sintering temperature has a dramatic effect on the electrode microstructure, which in turn will influence the electrode properties. Therefore, the microstructures of the NSF cathodes at each sintering temperature were studied. Figure 4 shows typical SEM images of NSF1010 electrodes after sintering at different temperatures for 2 h. It was observed that only poor contacts were formed between the NSF1010 particles when the sintering temperature was 950 °C (Fig. 4a). Sintering at 1,000 °C resulted in a structure with moderate porosity, and strong contacts between the NSF1010 electrode and the SDC electrolyte. The thickness of the electrode was about

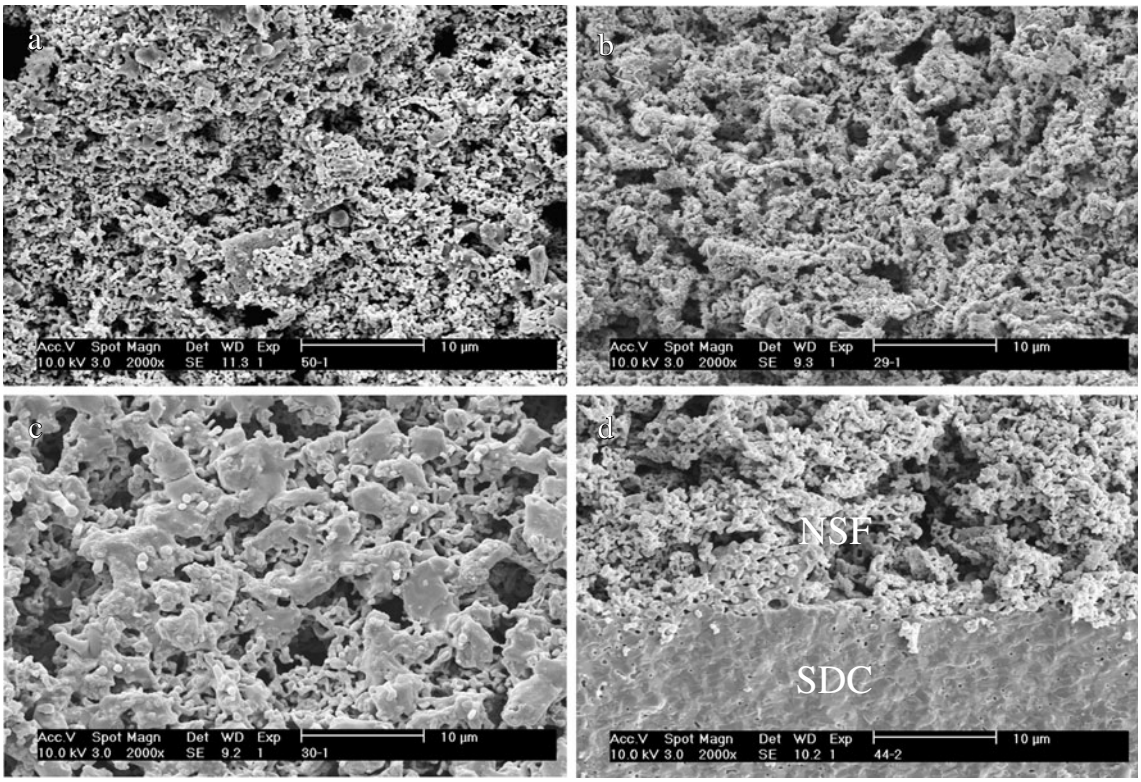

Fig. 4 SEM images of the surfaces of NSF1010 electrodes sintered at (a) 950 °C; (b) 1,000 °C; (c) 1,100 °C; (d) a cross-section image of the test cell

20 μm (Fig. 4b, d). When the electrode was sintered at 1,100 °C for 2 h, however, an oversintering phenomenon was observed (Fig. 4c). This effect decreased the electrode porosity and triple-phase boundary length, resulting in an increase in R_p. A similar effect has been reported in the literature [31]. On the basis of the above results, sintering at 1,000 °C for 2 h was chosen as a fixed parameter to obtain the best sintering performance for all subsequent studies.

The temperature dependence of polarization resistance for the $Nd_{2-x}Sr_xFeO_{4+\delta}$ (x=0.5, 0.6, 0.8, 1.0) materials is presented in Fig. 5. As can be seen from Fig. 5, the polarization resistance decreased with increasing Sr dopant content over the entire temperature range examined. This may be attributed to the loss of lattice oxygen and the formation of oxygen vacancies, a process enhanced by the Sr doping [32]. It was observed that NSF1010 showed the lowest polarization resistance of 2.75 Ω cm^2 at 700 °C in this experiment, similar to the values reported for $Ba_{2-x}Sr_xFeO_{4+\delta}$ and $Sm_{2-x}Sr_xCoO_{4+\delta}$ electrode materials [22, 25], but this is still higher than the resistances reported for well-known materials such as $La_{1-x}Sr_xCo_{1-y}Fe_yO_{3-\delta}$.

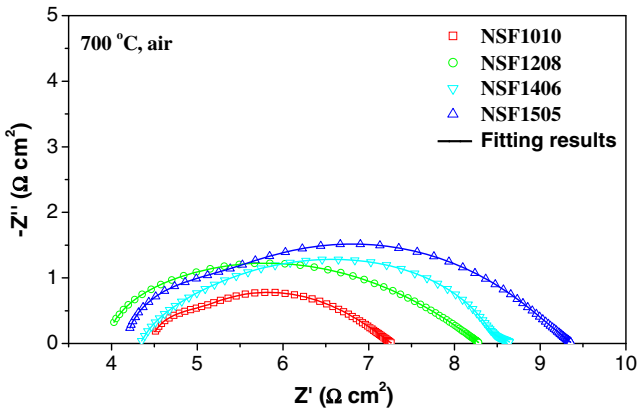

Fig. 5 Impedance spectra of $Nd_{2-x}Sr_xFeO_{4+\delta}$ (x=0.5, 0.6, 0.8, 1.0) cathodes at 700 °C under open-circuit potential in air

In order to clearly delineate the electrochemical process, the fitting results of these cathodes were calculated and are summarized in Table 1. The high-frequency resistance (R_1) is smaller than the low-frequency resistance (R_2), and the processes occurring in the higher frequency region proceed more rapidly than those occurring in the lower frequency region, implying that the oxygen reduction reaction is limited primarily by the oxygen adsorption or desorption process on the electrode surface. Arrhenius plots of R_1 and R_2 separated from the fitting results of the electrochemical impedance spectrum for the NSF1010 cathode are plotted in Fig. 6. The fitting data could be well formulated using the Arrhenius equation [33]. The apparent activation energy (E_a) values calculated from the slopes of the ln(T/R) versus 1,000/T plots are also included in Fig. 6. Based on the slopes of the fitting lines in Fig. 6, the E_a (98.1 kJ mol^{-1}) for the R_1 was smaller than the E_a (107.8 kJ mol^{-1}) for the

Table 1 Fitting polarization resistance extracted from the impedance of $Nd_{2-x}Sr_xFeO_{4+\delta}$ (x = 0.5, 0.6, 0.8, 1.0) cathodes at 700 °C

	Experimental data	Fitted resistance values of the different parameters		
	R_p (Ω cm^2)	R_1 (Ω cm^2)	R_2 (Ω cm^2)	$R_1 + R_2$ (Ω cm^2)
NSF1010	2.75	0.56	2.23	2.79
NSF1208	4.25	0.81	3.51	4.32
NSF1406	4.29	1.00	3.43	4.43
NSF1505	5.14	1.13	4.18	5.31

R_2. This result further demonstrates that it is the oxygen desorption or adsorption process that constitutes the rate-limiting step for oxygen reduction in these cathode materials.

According to the impedance data obtained at different test temperatures, the temperature dependence of the polarization resistance for the $Nd_{2-x}Sr_xFeO_{4+\delta}$ (x=0.5, 0.6, 0.8, 1.0) materials is plotted in Fig. 7. As can be seen from Fig. 7, the E_a values for NSF1010, NSF1208, NSF1406, and NSF1505 were 105.6, 118.6, 123.6, and 126.7 kJ mol^{-1}, respectively, similar to that of the $Ba_{2-x}Sr_xFeO_{4+\delta}$ electrode material reported by Jin et al. [25].

Cathodic overpotential is an important parameter for SOFCs. The cathodic overpotential as a function of current density at different temperatures is plotted in Fig. 8. At low overpotentials (less than 10 mV), we can expect a linear expression [34], $i=i_0ZF\eta/RT$, where i is the current density, i_0 is the exchange current density, η is the overpotential, F is Faraday's constant, and R is the universal gas constant. From the inverse of the derivative of i against η, we can obtain the area-specific resistance.

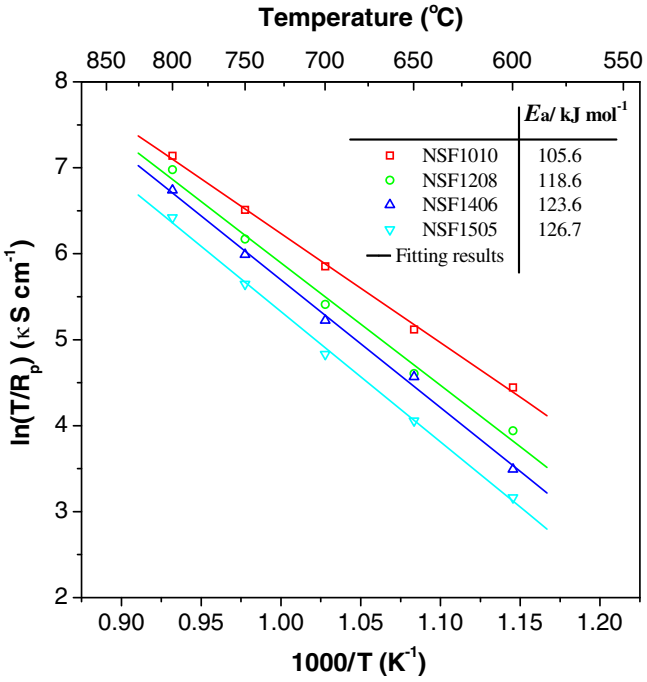

Fig. 7 Arrhenius plots of the polarization resistance for $Nd_{2-x}Sr_xFeO_{4+\delta}$ (x=0.5, 0.6, 0.8, 1.0) materials under open-circuit-potential conditions

The value obtained at 700 °C in air was 2.31 Ω cm^2, which is very close to the value obtained from the impedance measurements. It is evident from Fig. 7 that the current density increases with increasing temperature. It can be seen that the cathode overpotential was also affected by the Sr content. The increase in Sr content resulted in a significant reduction in the cathode overpotential in the experimental range. The lowest polarization overpotential of 68 mV was measured for an NSF1010 cathode at a current density of 24.3 mA cm^{-2} at 700 °C in air.

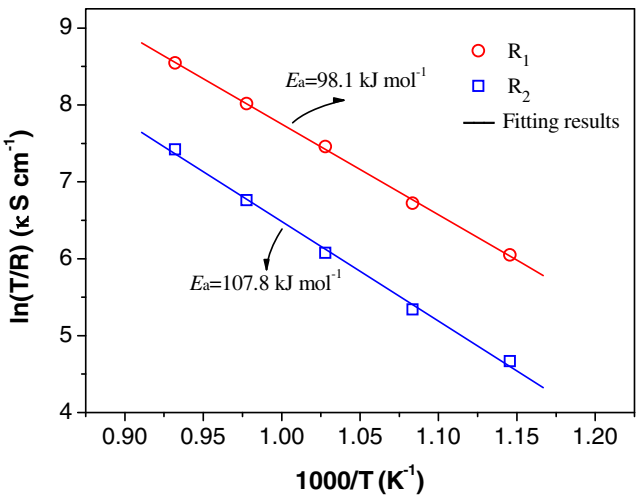

Fig. 6 Arrhenius plots of R_1 and R_2 separated from the fitting results of the electrochemical impedance spectrum of an NSF1010 cathode

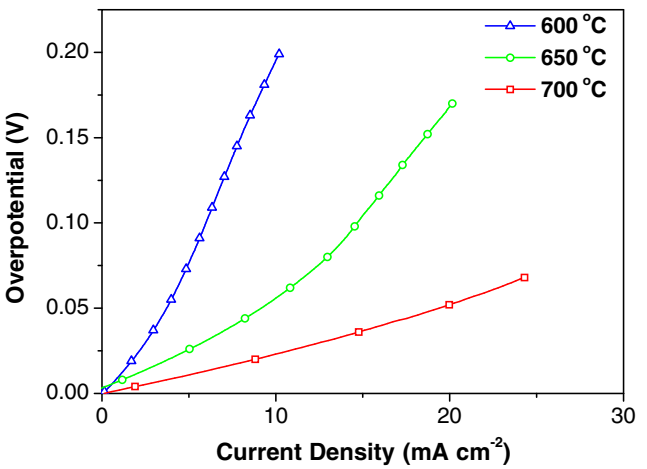

Fig. 8 Cathodic overpotential for NSF1010 at different temperatures as a function of current density

Conclusions

$Nd_{2-x}Sr_xFeO_{4+\delta}$ (x=0.5, 0.6, 0.8, 1.0) materials have been prepared and their potential as cathode materials for IT-SOFCs has been evaluated. All of the samples were obtained as a K_2NiF_4-type structural phase by the glycine–nitrate gel route. $Nd_{1.0}Sr_{1.0}FeO_{4+\delta}$ have been found to have good chemical compatibility with SDC electrolyte. The NSF cathode formed good contacts with the SDC electrolyte after sintering at 1,000 °C for 24 h. In the series $Nd_{2-x}Sr_xFeO_{4+\delta}$ (x=0.5, 0.6, 0.8, 1.0), $Nd_{2-x}Sr_xFeO_{4+\delta}$ showed the lowest polarization resistance of 2.75 Ω cm^2 at 700 °C. It was also found that the electrochemical properties were remarkably improved with increasing Sr content in the experimental range. The electrochemical impedance spectra revealed that the process ascribed to the low-frequency impedance arc (desorption or adsorption process) is the rate-limiting process for the oxygen reduction reaction in these cathode materials. According to the cathodic polarization results, at an overpotential of 68 mV, the maximum polarization current density of the $Nd_{1.0}Sr_{1.0}FeO_{4+\delta}$ cathode on SDC electrolyte at 700 °C was about 24.3 mA cm^{-2}. The present experimental results suggest that the studied system may have potential application as a cathode material for solid oxide fuel cells.

Acknowledgments The authors gratefully acknowledge financial support from the National High Technology Research Development Project of China (No. 2007AA05Z136), the National Natural Science Foundation of China (No. 20976063), the Key Project of the Ministry of Education of China (No. 210163), and the Natural Science Foundation of Guangxi Zhuang Autonomous Region (No. 2010GXNSFA013045).

References

1. Minh NQ (1993) J Am Ceram Soc 76:563–588
2. Adler SB (2004) Chem Rev 104:4791–4844
3. Zha SW, Moore A, Abernathy H, Liu ML (2004) J Electrochem Soc 151:A1128–A1133
4. Horita T, Yamaji K, Ishikawa M, Sakai N, Yokokawa H, Kawada T, Kato T (1998) J Electrochem Soc 145:3196–3202
5. Shao Z, Haile SM (2004) Nature 431:170–173
6. Esquirol A, Brandon NP, Kilner JA, Mogensen M (2004) J Electrochem Soc 151:A1847–A1855
7. Skinner SJ (2003) Solid State Sci 5:419–426
8. Vashook VV, Yushkevich II, Kokhanovsky LV, Makhnach LV, Kononyuk IF, Ullmann H, Altenburg H (1999) Solid State Ionics 119:23–30
9. Skinner SJ, Kilner JA (2000) Solid State Ionics 135:709–712
10. Kharton VV, Viskup AP, Kovalesky AV, Naumovich EN, Marques FMB (2001) Solid State Ionics 143:337–353
11. Zhao F, Wang X, Wang Z, Peng R, Xia C (2008) Solid State Ionics 179:1450–1453
12. Li Q, Zhao H, Huo L, Sun L, Cheng X, Grenier J-C (2007) Electrochem Commun 9:1508–1512
13. Chen SC, Ramanujachary KV, Greenblatt M (1993) J Solid State Chem 105:444–457
14. Solak N, Zinkevich M, Aldinger F (2006) Solid State Ionics 177:2139–2142
15. Fontaine ML, Laberty-Robert C, Ansart F, Tailhades P (2006) J Power Sources 156:33–38
16. Vashook V, Zosel J, Wen TL, Guth U (2006) Solid State Ionics 177:1827–1830
17. Mauvy F, Bassat JM, Boehm E, Manaud JP, Dordor P, Grenier JC (2003) Solid State Ionics 158:17–28
18. Lalanne C, Mauvy F, Siebert E, Fontaine ML, Bassat JM, Ansart F, Stevens P, Grenier JC (2007) J Eur Ceram Soc 27:4195–4198
19. Li Q, Fan Y, Zhao H, Sun LP, Huo LH (2007) J Power Sources 167:64–68
20. Vashook VV, Tolochko SP, Yushkevich II, Makhnach LV, Kononyuk IF, Altenburg H, Hauck J, Ullmann H (1998) Solid State Ionics 110:245–253
21. Ishikawa K, Kondo S, Okanc H, Suzuki S, Suzuki Y (1987) Bull Chem Soc Jpn 60:1295–1298
22. Wang YS, Nie HW, Wang SR, Wen TL, Guth U, Vashook V (2006) Mater Lett 60:1174–1178
23. Cao Y, Gu HT, Chen H, Zheng YF, Zhou M, Guo LC (2010) Int J Hydrogen Energy 35:5594–5600
24. Jennings AJ, Skinner SJ (2002) Solid State Ionics 152–153:663–667
25. Jin C, Liu J, Zhang YH, Sui J, Guo WM (2008) J Power Sources 182:482–488
26. Chick LA, Pederson LR, Maupin GD, Bates JL, Thomas LE, Exarhos GJ (1990) Mater Lett 10:6–12
27. Blank DHA, Kruidhof H, Flokstra J (1988) J Phys D Appl Phys 21:226–232
28. Gu HT, Chen H, Gao L, Zheng YF, Zhu XF, Guo LC (2009) Int J Hydrogen Energy 34:2416–2420
29. Li SY, Lü Z, Huang XQ, Su WH (2008) Solid State Ionics 178:1853–1858
30. Ding XF, Cui C, Guo LC (2009) J Alloy Compd 481:845–850
31. Zhao H, Huo LH, Sun LP, Yu LJ, Gao S, Zhao JG (2004) Mater Chem Phys 88:160–166
32. Tai LW, Nasrallah MM, Anderson HU, Sparlin DM, Sehlin SR (1995) Solid State Ionics 76:259–271
33. Kim S, Yang YL, Christoffersen R, Jacobson AJ (1997) Solid State Ionics 104:57–65
34. Steele BCH (1995) Solid State Ionics 75:157–165